Three dimensional optical manipulation and structural imaging of soft materials by use of laser tweezers and multimodal nonlinear microscopy

Rahul P. Trivedi,[1] Taewoo Lee,[1] Kris A. Bertness,[2] and Ivan I. Smalyukh[1,3,*]

[1]Department of Physics and Liquid Crystal Materials Research Center, University of Colorado, Boulder, Colorado 80309, USA

[2]

11. M. Yada, J. Yamamoto, and H. Yokoyama. "ōDirect observation of anisotropic interparticle forces in nematic colloids with optical tweezers.ö" Phys. Rev. Lett. **92**(18),

39. T. Lee, R. P. Trivedi, and I. I. Smalyukh."õMultimodal nonlinear optical polarizing microscopy of long-range molecular order in liquid crystals.ö"Opt. Lett. **35**(20), 3447ó3449 (2010).

40. The full description of the procedures used in this paper requires the identification of certain commercial products and their suppliers. The inclusion of such information should in no way be construed as indicating that such products or suppliers are endorsed by NIST or are recommended by NIST or that they are necessarily the best materials, instruments, or suppliers for the purposes described.

41. K. A. Bertness, A. Roshko, L. M. Mansfield, T. E. Harvey, and N. A. Sanford."õMechanism for spontaneous growth of GaN nanowires with molecular beam epitaxy.ö"J. Cryst. Growth **310**(13), 3154ó3158 (2008).

42. J. B. Schlager, K. A. Bertness, P. T. Blanchard, L. H. Robins, A. Roshko, and N. A. Sanford."õSteady-state and time-resolved photoluminescence from relaxed and strained GaN nanowires grown by catalyst-free molecular-beam epitaxy.ö"J. Appl. Phys. **103**(12), 124309 (2008).

43. J. Liesener, M. Reicherter, T. Haist, and H. J. Tiziani."õMulti-functional optical tweezers using computer-generated holograms.ö"Opt. Commun. **185**(1-3), 77ó82 (2000).

44. J. E. Curtis, B. A. Koss, and D. G. Grier."õDynamic holographic optical tweezers.ö"Opt. Commun. **207**(1-6), 169ó175 (2002).

45. J. E. Curtis, and D. G. Grier."õStructure of optical vortices.ö"Phys. Rev. Lett. **90**(13), 133901 (2003).

46. The notation such as BPF 417/60 denotes a bandpass filter with center wavelength of 417 nm and 60 nm bandwidth.

47. D. B. Conkey, R. P. Trivedi, S. R. P. Pavani

rod-shaped molecules whose local average orientation is described by the molecular director, **n**(**r**), which is also the local optical axis of these materials. LCs have found both fundamental and technological importance, e.g., in display and other electro-optic devices, and are also significant from biological standpoint as lipids, viruses, and membranes form LC phases [2ó6]. Introducing chirality in nematic LCs enriches the phase behavior by resulting in chiral nematic phases, viz., cholesteric and blue phases [1]. In the cholesteric LC, the molecules show a uniform twist along a helical axis, giving rise to a periodic lamellar-like ground state.

The inherent anisotropy of LC materials imparts unique properties to LC-based colloidal dispersions [7,8]. The elasticity- and defect-mediated interactions between colloids in LCs are markedly different from those between colloids dispersed in isotropic media, allowing for novel ways of nano-scale and micro-scale colloidal self-assembly. Optical manipulation, which has already marked its importance in the field of colloidal science [9] and biology [10], has attained a place of pivotal interest in probing these so-ecⅿgf"õNE"eqⅿqkfuö"]11ó17], and multitudes of other LC systems such as defect-structures [17ó21], Langmuir monolayers [22] and LC droplets [23,24]. Optical trapping has proved to be a valuable tool in determining the nature of interaction forces [11ó13], characterizing viscous drag on colloidal inclusions in LCs [25,26], controlling dynamics of trapped particles by use of direction-dependent optical trapping forces in LCs [15], probing defect topology [16,21], and characterizing line tension of disclination defects [18,19,21], etc. Optical manipulation in LCs is not restricted to tweezing of foreign inclusion but extends to manipulation of the director field **n**(**r**) with a focused laser beam ó leading to generation of localized defect structures [27] which, in turn, are amenable to optical tweezing.

While performing optical manipulation in LCs, it is imperative that the changes in **n**(**r**) effected by inclusion of colloids, or by application of external optical/electric fields, be imaged to elucidate the underlying physical phenomena. For example, characterization of anisotropic viscoelastic properties of LCs using active microrheology assisted by laser tweezers is complicated by the fact that the probe particles typically induce topological defects and distortions of long-range molecular alignment [15,25,26], which need to be visualized to provide a deeper understanding of the nature of ensuing colloidal interactions. The conventional technique of optical polarizing microscopy reveals the depth-averaged **n**(**r**) kp"vjg"ncvgtcn"rncpg"rgtrgpfkewnct"vq"vjg" oketqueqrgøu"qrvkecn"czku0"Kv"ku"qhvgp"k o rquukdng"vq" deduce the full three-dimensional (3D) **n**(**r**) from this. Combination of optical manipulation with 3D imaging technique such as fluorescence confocal polarizing microscopy (FCPM) [28ó31] has enabled substantial progress in LC imaging. This approach however requires the LC to be doped with fluorescent dyes whose molecules align along the local **n**(**r**) without distorting it. For certain imaging applications such as imaging of some biological systems or characterization of pre-packaged devices, introduction of dyes is precluded, as it may either be obtrusive to their natural functioning or undesired for their successive application. Hence, several nonlinear optical microscopy techniques have been used for imaging of **n**(**r**) in LCs: viz., coherent anti-Stokes Raman scattering (CARS) [32ó34], four-wave mixing [35], second-harmonic generation (SHG) [36], third-harmonic generation [37], three-photon excitation fluorescence (3PEF) [38], etc. These techniques, and also multimodal nonlinear optical polarizing microscopy (MNOPM) that combines multiple nonlinear optical imaging modalities [39], address this issue by directly probing the ordered arrangement of constituent molecules or building-blocks of the LCs instead of relying on additives such as dyes. However, simultaneous implementation of these 3D imaging techniques with 3D optical manipulation has never been demonstrated. We show here the simultaneous use of holographic optical trapping (HOT) with the MNOPM imaging system. MNOPM includes imaging modalities such as CARS, multi-photon excitation fluorescence (in particular, we show imaging performed in 3PEF), and multi-harmonic generation (with the example of imaging in SHG). This integrated system gives capabilities of non-contact 3D optical manipulation along with non-invasive, label-free, high resolution and orientation sensitive 3D imaging.

2. Experimental

2.1 Optical setup

The schematic diagram of the integrated MNOPM and HOT system is shown in Fig. 1. The two systems are coupled to an inverted microscope (IX-81, Olympus [40]). A tunable (680-1080 nm) Ti-Sapphire oscillator (140 fs, 80 MHz, Chameleon Ultra II, Coherent) is used as the primary excitation source for the nonlinear optical imaging modalities. For CARS imaging, the femtosecond pulse at 780 nm is split into two arms: the pump/probe beam and the other beam which synchronously pumps a highly nonlinear, polarization maintaining photonic crystal fiber (PCF, FemtoWHITE-800, NKT photonics). The broadband Stokes pulse is derived from the supercontinuum output of the PCF (spanning a range from ~550nm to ~1600 nm). The two beams are recombined at a filter (BLP01-785R-25, Semrock Inc.) that spatially overlaps the pump/probe pulse (at 780 nm) and the broadband Stokes pulse (consisting of the part of the supercontinuum above 785 nm). The temporal overlap of the two pulses is ensured by adjusting delay lines in each arm, before directing them into the galvanomirror-based scanning unit (Fluoview FV300, Olympus). For SHG and 3PEF, the pulse is shunted directly into the scanning unit. The excitation light is focused into the sample by use of a high numerical aperture (NA) objective lens (100x, oil-immersion, NA = 1.4, Olympus) and collected by another objective (60x, oil-immersion, NA = 1.42, Olympus) in forward mode or the same one for detection in epi-mode. The nonlinear signals are detected with photomultiplier tubes (H5784-20, Hamamatsu) after passing through a series of dichroic mirrors and bandpass filters. A Faraday isolator is used to protect the Ti:Sapphire laser from the back-reflection of the PCF, and a combination of a half-wave plate and a Glan laser polarizer allows us to control power and polarization of the laser. The pulse is passed through a dual prism dispersion compensator before it is split. A laser line filter (LL01-780, Semrock Inc) is used to reduce the spectral bandwidth of pump/probe pulses for suppressing the non-resonant background signal in the CARS imaging mode. All spectra are measured at forward detection position by an optical fiber ó coupled spectrometer (USB2000-FLG, Ocean Optics).

The HOT system (see Fig. 1) is built around a reflective, electrically addressed, phase-only, liquid crystal spatial light modulator (SLM, Boulder Nonlinear Systems) with 734" "734" rkzgnu."gcej"qh"uk|g"37" "37" o0"Tghtguj"tcvg"qh"37" J |"hqt"vjg"eqo rwvgt-generated holograms supplied to the SLM ensures real-time manipulation. The trapping system employs a continuous-wave Ytterbium-doped fiber laser at 1064 nm (YLM-10, IPG Photonics). The polarization of the beam incident on the SLM is tuned to maximize the phase modulation efficiency of the SLM by use of a Glan laser polarizer and a half-wave plate. The first telescope (lenses L1 and L2) expands the beam-size to slightly overfill the active area of the SLM. The second telescope, in 4f configuration (lenses L3 and L4), projects the SLM onto the back-aperture of the objective while also resizing the beam to overfill the latter. The holographic nature of the trapping system enables movement of traps and manipulated objects pqv"qpn{"kp"vjg"vtcpuxgtug"rncpg"dwv"cnuq"cnqpi"vjg" oketqueqrg¢u"qrvkecn"czku0"C   u   to   t

Fig. 1. Schematic diagram of the integrated MNOPM and HOT optical setup which is built around an inverted microscope. The components of MNOPM: HWP: half wave-plate, GLP: Glan-laser polarizer, PCF: photonic crystal fiber, AL: aspheric lens, BS: beam-splitter, BC: beam combiner, FM: folding mirror, PMT: photo-multiplier tube, DM: dichroic mirror, OL:

[(1 1 0 0) family], producing the hexagonal cross-section. The nanorods are first dispersed in isopropanol and then transferred into the LC by mixing and letting isopropanol evaporate by heating the mixture to ~60 °C.

3. Results

3.1 Optical manipulation and nonlinear imaging of colloids in LC host media

HOT has found numerous applications in materials and biological sciences because of its ability to manipulate multiple objects simultaneously in 3D [43,44] as well as in allowing the generation of laser trapping beams with optical vortices [45]. We demonstrate 3D manipulation and nonlinear imaging capabilities of the integrated setup by using an example of a system consisting of cholesteric LC as the host medium and colloids of spherical and anisometric (rod-like) shapes dispersed in it.

Fig. 2. Manipulation and imaging of spherical microparticles in a cholesteric LC. Images show vertical cross-sections of planar cholesteric LC cells obtained in 3PEF (a-c) and CARS (d-f) modes, displaying the cholesteric lamellae having spherical microparticles embedded within them. Particles of 4

cell thickness, and are partially suppressed in the images shown by the strong tangential boundary conditions for layer orientation at the cell substrates.

In general, motion of particles perpendicular to the layers is more difficult compared to that within a layer. The HOT system allows motion of particles along the optical axis of the microscope [direction z, Fig. 2(a)], i.e., across the cholesteric layers at relatively high values of optical power (~50 mW, compared to ~10 mW sufficient to move the particles laterally). Due to the high NA of the objective used, the range of movement along z attainable by HOT is limited to only a few microns. In the case of the images shown, a large range of particle displacements (tens of micrometers) along z zT e s   4 ( ) 4 (

                                                        a n d   - 3 6 [(t

                                                ,   J L W K H   D

                                            ,

                                            ,

has a non-singular structure of the defect core [16]. Since **n**(**r**+"kp"vjg"eqtg"qh"vjg" -disclination is along the disclination, the nanorod prefers to align along the defect line.
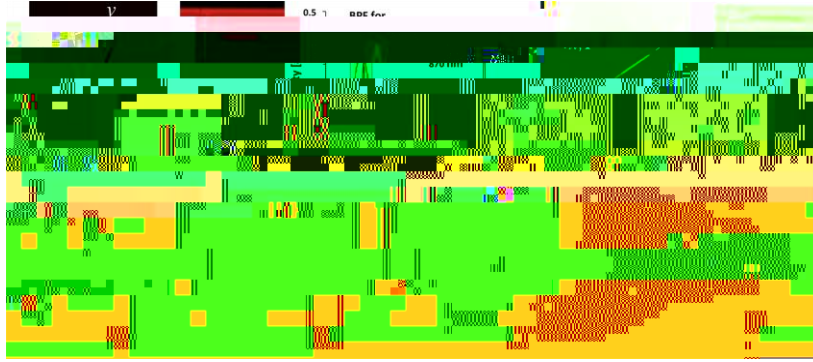

Fig. 3. 3D Imaging of GaN nanorods dispersed in a cholesteric LC. GaN nanorods are manipulated in the layered structure of the cholesteric LC and the LC-nanorod composite is imaged in its lateral plane as well as in the vertical cross-section in two nonlinear modes: the LC is probed using 3PEF (a, b) and CARS (d, e) and the nanorods are visualized in SHG. (c) shows the spectrum with the excitation at 870 nm and the 3PEF emission from the LC molecules and SHG (at 435 nm) from the GaN nanorods. The nanorods interacting with a cholesteric dislocation are imaged in 3PEF (f-h). (g) shows 3PEF image of a dislocation eq o r tkukpi" $^{+1/2}$ cpf" $^{-1/2}$ disclinations in its vertical cross-section. The schematic diagram of the molecular director pattern around the dislocation with the position of the nanorod embedded in it is shown in (i).

3.2 Optical generation of LC defect structures

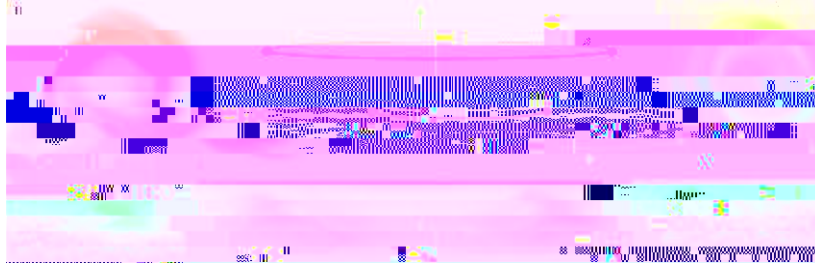It has been long known that LCs respond to an applied electric field (the so-called Freederickz

Fig. 4. 3D imaging of optically generated defect structures in a homeotropic unwound cholesteric LC sample. Loops of cholesteric finger CF-1 are optically generated with the HOT setup and are imaged in their lateral and vertical cross-sectional planes, in 3PEF (a,d) and CARS (c,e) imaging modes. The schematic representation of the twist of $\mathbf{n(r)}$ within the structure is shown in its vertical cross section (b). The red dots and lines represent the loop of pqpukpiwnct fkuenkpcvkqpu $^{+1/2}$ yjkng vjg dnwg fqvu cpf nkpgu eqttgurqpf vq $^{-1/2}$ disclination loops. The structure is axially symmetric around the axis marked by the green double arrow.

4. Discussion

4.1 Comparison of the integrated system with other imaging and trapping approaches

Optical manipulation has proved to be a tool of immense utility in quantifying elasticity-

detection polarizer collinear with polarization of excitation beams) [33,39]. These stronger dependencies on compared to FCPM impart an enhanced sensitivity to spatial variations in $\mathbf{n}(\mathbf{r})$ in all MNOPM imaging modalities. FCPM imaging of LCs with twisted configurations of $\mathbf{n}(\mathbf{r})$, with the helical axis parallel to the microscorgøu" czku" ku" fkhhkewnv." dgecwug" vjg" polarization of the imaging light follows the twist of $\mathbf{n}(\mathbf{r})$ as it propagates through the LC. This so-called Mauguin effect is quantified by the Mauguin parameter, $_{Mauguin}$, where p is the pitch of the twist in $\mathbf{n}(\mathbf{r})$ structure being imaged, is its birefringence and is the wavelength of imaging light. Large values of $_{Mauguin} \gg 1$ are detrimental to imaging and preclude the reconstruction of $\mathbf{n}(\mathbf{r})$. MNOPM partially mitigates this issue, as is in the near-infrared range. The use of longer excitation wavelengths in MNOPM imaging also helps improve the penetration depth inside the sample compared to FCPM (Table 1). The defocusing because of scattering due to fluctuations of $\mathbf{n}(\mathbf{r})$ is also less severe for longer wavelengths. By using short-pitch cholesteric LCs and comparing the FCPM and MNOPM images of sub-micrometer cholesteric structures having both vertical and horizontal layers, we find that MNOPM imaging modalities offer somewhat better radial and axial spatial resolution, owing to inherently localized excitation of nonlinear optical signals (Table 1) despite the wavelength of their excitation being in the near-IR range.

Table 1. Comparison of different orientation-sensitive 3D microscopy techniques

Microscopy technique	3D spatial resolution*	Dye labeling	Orientational sensitivity	Mauguin effect	Penetration depth

speed of imaging [33]. The optical forces exerted by the imaging beam (both gradient and scattering forces) on the colloidal particles or director structures can be a significant source of unintended optical manipulation when high optical power and slow rate of beam scanning are used. For the imaging reported here, the optical power at the sample is small enough (combined power < 2 mW) so that effects due to the optical Freederickz transition as well as those due to optical forces are negligible.